

PRECISE MODELING OF ARCHEOLOGICAL ARTIFACTS

Junta Doi, Wataru Sato, Masahiko Hoshi, Shinji Morishita, Tomohiro Morita, Kota Sudo, Youhei Nakanishi
Chiba Institute of Technology, Department of Computer Science

Keywords: Matrix format data structure, Topology assigned modeling, 3D shape processing, Archeological artifact, Depth-to-depth transformation operator.

Abstract: Precise shape reconstruction of archeological artifacts within 0.01 mm 3D resolutions are reported based on our proposal of a practical, accurate, topologically robust and ranging error resistive shape modeling procedure that approximates a real 3D object, with the matrix-format data structure, for the resulting shape processing. Examples of the shape processing are based on the premise of the virtual manipulation of the 3D shape. Radial distance of each scanning point is measured by laser triangulation. A face array listing, which defines the sampling point connectivity and the shape of the mesh, is assigned to meet the desired meshing. Topologically stable meshing, and hence, an accurate approximation, free from the shape ambiguity unavoidable in the so-called ICP (Iterative Closest Point) modeling, is then accomplished. This proposal allows not only the precise shape modeling, but also virtual shape manipulation for various trainings and restorations.

1 INTRODUCTION

Attempts to measure the shape of objects and to construct geometric models have a long history. There are a great number of books, review articles (Scott et al., 2003; and Blais, 2004), papers (Turk et al., 1994; Levoy et al., 2000; Rusinkiewicz et al., 2001; Godin et al., 2002; and Pauly et al, 2003), and products (Simple3D, 2005) dealing with the problems.

This study is to provide technology that would reconstruct the objects, such as, archeological artifacts accurately and precisely as they are in a usually noisy environment. A 3D shape processing for restoration is another purpose of the proposal.

Surface models with unorganized triangular meshes were built based, for instance, on the so-called ICP algorithm, from triangulation scanners so far. The ICP algorithm is well proven; however, it is noise-sensitive and hence, shape ambiguity becomes unavoidable. In general, the presence of noise is typical for the scanning process. Retrieving the surface topology from the surface geometry as the algorithm is a difficult problem, especially when the ranging noise is unavoidable. Many attempts have been made to overcome the problem; however, there is no known algorithm that has theoretical guarantees, without any assumptions, in the presence of noise (Dey et al., 2004). Most scientific efforts are toward the unorganized meshing. Contrary to the procedures,

topology is first assigned in our procedure, enabling the matrix-format organized meshing and versatile 3D shape processing.

The ranging noise arises mostly from the oblique reflection of the incident laser beam on the local surface. In the 3D shape modeling procedure, this noise problem is serious and inevitable. However, few articles discussed the problem. To reduce the noise, a large object model with rather flat surfaces is to be employed. The surface polishing is most effective for a reliable triangulation. These measures are, however, not applicable to most of the objects that should be treated as they are.

Successive shape modification is applied to the organized and point-locatable model using intuitive matrix-type operators enabling the quantitative shape evaluation and CAD compatibilities.

2 MODELING AND SCANNING

In an illustration of a solid model data structure in Fig. 1, a pentahedral volume element, in which the peripheral surface is covered with a rectangular mesh, small enough to approximate the curved object surface, is to be measured to approximate the object shape. A quadrilateral mesh S_a , consisting of four surface points, a , b , c and d , is one of the sampling points on the object surface. Points A , B , C and D are mesh points consisting of a rectangular mesh SA on the unit

cylinder surface. The rectangular mesh SA is a perspective projection of the quadrilateral mesh Sa to the unit cylinder surface, and vice versa. Each radial distance of the object surface point from the axis of rotation (z- axis), for instance, “ra, rb, · ·” is sequentially measured.

A vertex array listing, which is called “geometry” and represents the geometric coordinate values in 3D space is shown in Table 1. The face (mesh) array listings for the Sa and SA are shown in Tables 2. Four other surfaces comprised of the wedge shaped pentahedral volume element are similarly defined (tables not shown).The listing is called “topology” and defines the shape of the face (number of vertices or edges) and also defines the listing sequence of the vertices or connectivity. The listing sequence of the vertices in the face list defines the normal vector direction of the face and determines on which side of the face the solid part of the object exists.

As shown in Fig. 1 and Table 2, the variation in the radial distance of a, in principle, has no effect on the connectivity array of the face, if point a locates along the radial line segment O1-a or O1-A. This relation is also valid for the other points b, c, and d. Therefore, the connectivity array of the mesh is conserved if the four points similarly locate along each radial line. The vertex connectivity of Sa is the same as that on the unit cylinder, SA as shown in Fig. 1 and Table 2. This means that the face array listing assigned for the unit surface SA is valid for the object surface Sa. If every radial distance is large enough, the surface shape becomes totally planar. This procedure is valid for planar surface as well.

Our data format is a raster scan type or a matrix format as described above and it is as follows.

$$r = [r_{ij}] = \begin{bmatrix} r_{11} & r_{12} & \Lambda & r_{1m} \\ r_{21} & r_{22} & \Lambda & r_{2m} \\ M & M & O & M \\ r_{n1} & r_{n2} & \Lambda & r_{nm} \end{bmatrix} \quad (1)$$

An element r_{ij} represents the radial distance of a sampled surface point at the angular position “j” and at the vertical position “i” in the scanning This matrix can easily locate an arbitrary point on the object only by specifying “i” and “j.”

The same matrix-formatted shape modifying operators or depth-to-depth operators are applicable. An example of the 128x128 positive depth-to-depth operator is shown in Fig. 2 (left). Another example of the versatile operator is shown in Fig. 2 (center and right). A bread arc-board (center) and a customized depth-to-depth operator (right), which may be one of our modeled results, are shown. The operator shape can be pressed on the 3D models to make its replica. Bit-map characters and symbols are printed on any 3D

geometric models. The geometric models are fused

Table 1: Vertex array listing (geometry) for the quadrilateral surface meshes SA (left) and Sa (right) in Fig. 1.

Vertex	r	θ	z
SA: A	1	0	z1
B	1	θ	z1
C	1	θ	z2
D	1	0	z2
Vertex	r	θ	z
Sa: a	ra	0	z1
b	rb	θ	z1
c	rc	θ	z2
d	rd	0	z2

Table 2: Face array listing (topology) for the meshes SA (top) and Sa (bottom).

Face	1	2	3	4
Sa	a	b	c	d
SA	A	B	C	D

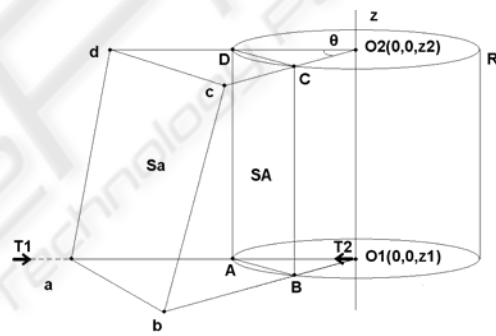


Figure 1: The mesh structure of the solid model cylinder. The points a, b, c, and d are scanned points on the object surface, while the points A, B, C and D are on the unit cylinder. The mesh ABCD is a perspective projection of the object surface mesh abcd on the unit cylinder surface, and vice versa. Variation in the radial distance of point “a” has no effect on the vertex connectivity of the mesh Sa, if “a” locates along the “O1-A.” This is valid for other three points. Scanning is aligned to successively follow the rectangular mesh SA. “T1” is the triangulation sensor.

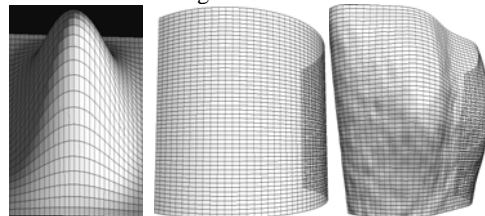


Figure 2: A positive depth-to-depth transformation operator (128x128 meshes, left). A bread arc-board (centre), instead of the planar board, and a customized 3D operator, which may be a thus reconstructed model of the real object. Convolution of the reconstructed model operator fuses two 3D shapes together.

together with the 3D operators by convolution.

An object such as a statue is placed on a turntable which is driven by a geared pulse motor with angular resolution of 0.02 degrees. This means that the horizontal (peripheral or horizontal) resolution is 0.015 mm at the radius of 43 mm and there are a maximum of 18,000 horizontal meshes in one 360 degree turn. The translational resolution of the vertical slider, which is also driven by a geared pulse motor, is 0.001 or 0.015 mm with a maximum stroke of 500 mm. There are 33,333 or 50,000 vertical meshes at maximum in the full stroke. Therefore, the maximum number of the quadrilateral meshes is 600 or 900 million.

A triangulation sensor with a diode laser is installed on the vertical slider. The spot size on the object surface is 0.3 or 0.1 mm in diameter. A sensing range from 250 mm to 750 mm at maximum is produced here with a resolution of 0.001 mm at best. In the procedure, the measurement is general and not limited to this type of sensing. As a modeling/rendering system, we prepared solid model interfaces for the popular 3D computer graphics and computer-aided design systems.

3 RESULTS AND DISCUSSION

The desired meshing, for instance, the rectangular SA is first assigned for the sampling point connection and then the vertex array listing is continuously updated. Our procedure results in the “B-reps” model, which describes a 3D object as a set of the organized quadrilateral meshes.

A replica of an Egyptian relief is modeled as shown in Figs. 3 and a fossil trilobite in Fig. 4. Other replica examples are: a human skull in Fig. 5, the Parthenon frieze in Fig. 6, and the Greek cavalier in Fig. 8. In these modeling, if the triangulation errors are detected, depth-to-depth transformation operators ($\mathbf{A} = [\mathbf{a}_{ij}], i=j=3, 5 \text{ or } 7$) are applied to the data matrix (1) to smooth the local surface or the noisy points are replaced with the surrounding data. This type of shape modifying operations, including a transcription example in Fig. 7 and shape modification in Figs. 9 and 10, are applicable only if the output data is a matrix-format as this procedure. The noise-eliminated model is also observed to closely follow the shape of the real object.

The matrix type data is convenient and essential for modifying a local shape when locating the target position. In Figs. 9 and 10, a bruise on the right cheek is modified to try to restore and the broken nose is similarly restored. These are supposing the restoration of a broken or damaged artifact or for virtual training of, for instance, cosmetic surgery.



Figure 3: A photograph and the shaded images of the reconstructed model (right) of an Egyptian relief. Horizontal and vertical resolutions are 0.01 mm and 0.015 mm, respectively. Depth resolution is 0.001 mm.

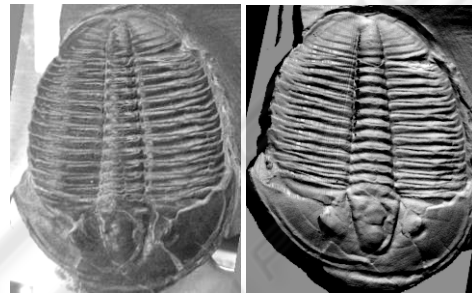


Figure 4: A photograph (left) and the shaded image of the modeled result of a fossil trilobite (right). Spatial resolutions are 0.01 mm both in horizontal and vertical directions. Depth resolution is 0.001 mm.



Figure 5: A photograph (left) and the shaded image of the modeled result of a plaster skull (right). Resolutions in rotational direction is 0.02 deg. and in vertical 0.015 mm.

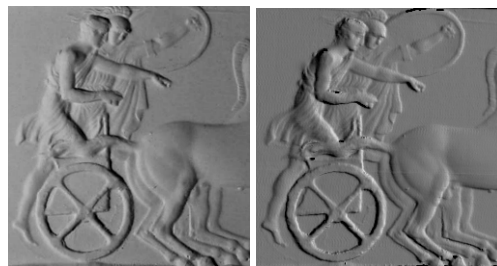


Figure 6: A photograph (left) and the shaded image of the modeled (left) of the Parthenon frieze, Charioteers replica (The British Museum). Resolutions in horizontal and vertical directions are 0.01 mm. Depth resolution is 0.001 mm.

The modeling accuracy depends on the rotational and translational positioning, and distance-sensing. The mal-aligned positioning results in a shape distortion, but still generates topologically stable models.

4 CONCLUSIONS

Some precise 3D models, within 0.01 mm 3D resolutions, are demonstrated based on the topology-assigned modeling procedure. The simple, automatic, geometrically accurate and precise, topologically stable, robust and noise-resistive object modeling, with matrix-format meshes, for archeological and cultural heritage applications. The noise problem inherent in the triangulation scanning, fatal in the so-called “retrieve topology from geometry” algorithm, is solved using the matrix format operators for practical usage in the exchange for some spatial resolution reduction. We expect considerable utility in the practical approximation and 3D shape processing.

REFERENCES

- Blais, F., 2004, Review of 20 Years of Range Sensor Development, *Journal of Electronic Imaging*, 13 (1), 231-240.
- Dey, T., Goswami, S., 2004, Provable Surface Reconstruction from Noisy Samples, Annual Symposium on Computational Geometry, In *Proceedings of 20th Annual Symposium on Computational Geometry*, 330-339.
- Godin, G., Beraldin, J., Taylor, J., Cournoyer, L., El-Hakim, S., Baribeau, R., Blais, F., Boulanger, P., Domey, J., Picard, M., 2002, Active Optical 3D Imaging for Heritage Applications *IEEE Computer Graphics and Applications*, 22, 24-36.
- Levoy, M., Pulli, K., Curless, B., Rusinkiewicz, S., Koller, D., Pereira, L., Ginzton, M., Anderson, S., Davis, J., Ginsberg, J., Shade, J., Fulk, D., 2000, The Digital Michelangelo Project; 3D Scanning of Large Statues, In *Proceedings of Siggraph 2000*, 131-144.
- Rusinkiewicz, S., Levoy, M., 2001, Efficient Variants of the ICP Algorithm, In Proceedings of the 3rd International Conference on 3-D Digital Imaging and Modeling (3DIM '01), 145-152.
- Scott, W., Roth, G., Rivest, J., 2003, View Planning for Automated Three-Dimensional Object Reconstruction and Inspection, *ACM Computing Surveys*, 35(1), 64-96.
- Simple3D, 2005, 3D Scanners, Digitizers, and Software for Making 3D Models and 3D Measurements, <http://www.simple3d.com/>
- Pauly, M., Keiser, R., Kobbelt, L., Gross, M., 2003, Shape Modeling with Point-Sampled Geometry, *ACM*

Transactions on Graphics (TOG), 22 (3), Special issue: *Proceedings of ACM SIGGRAPH*, 641-650.

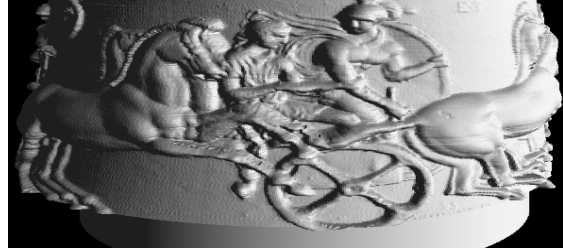


Figure 7: The modeled frieze replica in Fig. 7 is transcribed onto a cylinder on the supposition of a vase design. The left part of this figure corresponds with that of Fig. 6.



Figure 8: A photograph (left) and the shaded image of the modeled result (right) of a plaster statue (Greek cavalier Rampin). Resolutions are similar to those in Fig. 5.



Figure 9: The cheek bruise in the model in Fig. 8 is restored using similar operators in Fig. 2 (left). The plump (left) and the sunken cheeks (right) are depicted.



Figure 10: The cheek bruise and the broken nose are restored. The nose is restored by implanting another nose in a Greek mask and then shape modified using a depth-to-depth transformation operator in Fig. 2 (left). As the data structure is matrix-format, detailed procedures are not shown here.